Electric-Field-Tunable Spin Polarization and Carrier-Transport Anisotropy in an A-Type Antiferromagnetic van der Waals Bilayer

Wen Dang,[1,‡] Mengyu Zhu,[1,‡] Ziye Zhu,[2] Xiaofang Chen,[1] Zhigang Song,[3,*] and Jingshan Qi[1,†]

[1] *School of Physics and Electronic Engineering, Jiangsu Normal University, Xuzhou 221116, People's Republic of China*

[2] *School of Engineering, Westlake University, Hangzhou 310027, People's Republic of China*

[3] *John A. Paulson School of Engineering and Applied Sciences, Harvard University, Cambridge, Massachusetts 02138, United States of America*

(Received 17 August 2022; revised 14 November 2022; accepted 28 November 2022; published 28 December 2022)

Two-dimensional (2D) magnetic semiconductor materials with the electric-field-tunable spin polarization and carrier-transport anisotropy are of great significance for the fundamental physics and device application. Here we propose a general strategy to tune the spin polarization and anisotropic effective mass in a 2D A-type antiferromagnetic (AFM) bilayer system. We take the A-type AFM bilayer CrSBr (with the intralayer ferromagnetic and interlayer AFM coupling) as an example to confirm this design principle. Firstly, a vertical electric field can lift the spin degeneracy in the A-type AFM bilayer CrSBr. By flipping the direction of electric field, the spin polarization direction can be reversed. Secondly, in the A-type AFM bilayer CrSBr with an interlayer twist angle of 90°, both the spin direction and the carrier-transport anisotropy can be tuned simultaneously by applying a vertical electric field due to the in-plane anisotropic carrier effective mass in each CrSBr monolayer. This opens an opportunity for controlling the spin polarization as well as carrier-transport anisotropy in the 2D magnetic van der Waals layered materials by interlayer twist and electric field, and provides an idea for utilizing A-type AFM semiconductors to design spintronic devices.

DOI: 10.1103/PhysRevApplied.18.064086

I. INTRODUCTION

The rapid development of information technology requires the high integration, fast response, and small size of devices [1]. Spintronics [2] provides a superior platform for the information processing with the high data reading and writing speed and integration density by utilizing the spin degree of freedom, which has attracted wide attention [3–8]. Theoretically, the reduction of material dimension will lead to the enhancement of magnetic fluctuation, affecting the stability of the spin order in materials. Therefore, it is always controversial to obtain the long-range magnetic order in the low-dimensional systems [9]. In 2017, however, researchers observed the long-range magnetic order in the two-dimensional (2D) van der Waals (vdW) magnetic materials $Cr_2Ge_2Te_6$ [4] and CrI_3 [3]. This opens a door to develop 2D spintronics based on 2D magnetic materials [10]. To date, most spintronic devices are based on the ferromagnetic (FM) materials [11–13]. Since the antiferromagnetic (AFM) materials have some advantages, such as the robustness against magnetic field disturbances, high Néel temperature, ultrafast dynamics and no stray field [14], they become the candidates for next-generation spintronics. Thus, 2D AFM spintronic devices have potential applications in the future.

2D magnetic semiconductors with electrically tunable spin polarization are of great significance for both the fundamental physics and spintronic applications. It is still, however, a challenge to realize the control of spin polarization by an electric field in the existing low-dimensional materials. The concept that using an electrical field to break the symmetry of the AFM bilayer to achieve spin splitting of band structures has been proposed in vdW bilayer $MnPSe_3$ [15]. In a recent theoretical report, a spin half-metal is predicted in a 2D AFM 2H-VSe_2 bilayer by applying an electric field [16]. The unipolar and bipolar magnetic semiconductors with the electrically tunable spin polarization are also predicted theoretically in the A-type AFM bilayer semiconductor $NiBi_2Te_4$ and $Cr(pyz)_2$ [17]. In addition, the electrical polarization has been demonstrated to be able to modify valley properties in A-type vdW heterostructure [18]. Here, we propose a general strategy to realize the electric field control of the spin polarization and carrier transport anisotropy in an AFM bilayer semiconductor. We take bilayer CrSBr as an example to

*zhigangsong@seas.harvard.edu
†qijingshan@jsnu.edu.cn
‡These authors contributed equally to this work

 © 2022 American Physical Society

confirm the proposed strategy. This opens an opportunity for utilizing A-type AFM semiconductors to design spintronic devices by combining the interlayer twist and external electric field.

II. METHODS

A. First-principles atomistic and electronic structure calculations

Our studies are based on the first-principles calculations within the framework of density-functional theory (DFT) [19,20] as encoded in the Vienna *ab initio* simulation package (VASP) [21]. We use the Perdew-Burke-Ernzerhof (PBE) [22] functional to deal with the exchange-correlation interaction. The interaction between ions and electrons is described by a pseudopotential in basis set of the projector-augmented wave (PAW) [23]. We employ $3d^5 4s^1$ of Cr, $3s^2 3p^4$ of S, $4s^2 4p^5$ of Br as the valence electrons. The energy cut off is set to 250 eV. The Monkhorst-Pack method [24] is used for Brillouin-zone sampling with the a $11 \times 9 \times 1$ k-point mesh. The Hubbard U correction method [25] is used, where $U = 4$ eV is added to the Cr-d orbital. We check U from 1 to 5 eV and find the negligible influence on band structures [26]. For the bilayer CrSBr, we use Grimme's semiempirical correction method, DFT-D2 [27] to include the vdW interaction of the system. A large vacuum thickness (30 Å) along the c axis is adopted to avoid the interaction between adjacent unit cells. The total energy convergence is set as 1×10^{-7} eV. Both the lattice constants and the positions of all atoms are fully relaxed until the forces on all atoms are less than 0.001 eV/Å.

B. Carrier effective mass

The carrier effective mass is calculated by

$$m^*_{\alpha\beta} = \pm \hbar^2 \left(\frac{d^2 E}{dk_\alpha dk_\beta} \right)^{-1},$$

where k is the wave vector, and $\hbar$ is the reduced Planck constant. We calculate the effective mass within the orthogonal representation with the crystal axis of a and b, as shown in Fig. 1. Electron and hole effective mass of bilayer

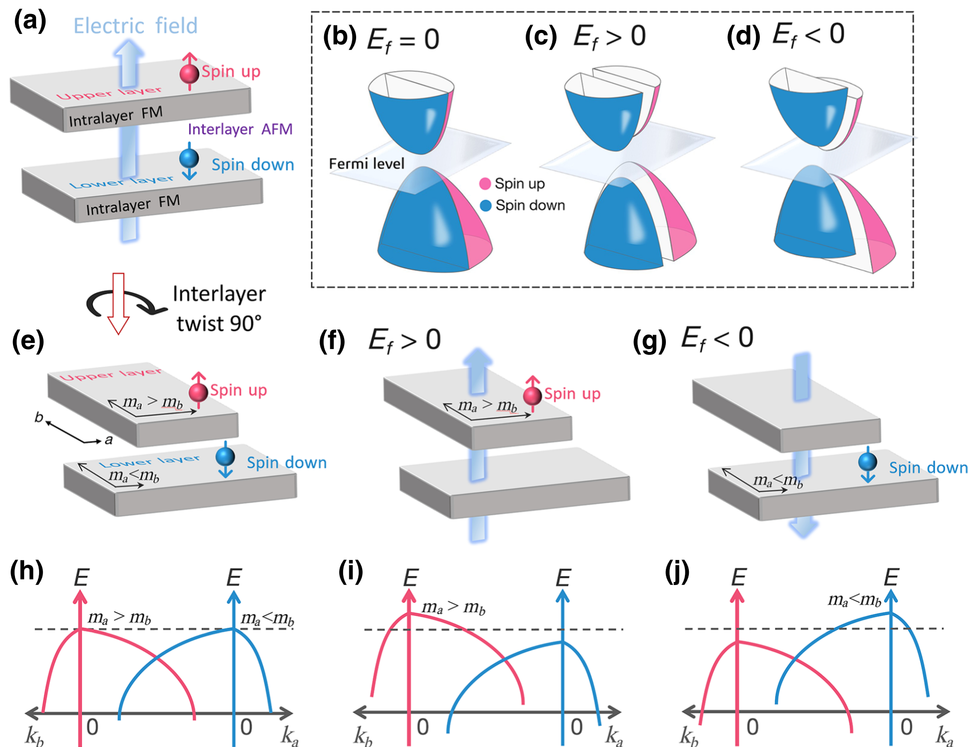

FIG. 1. Schematic principle of the electric field control of the spin polarization and carrier-transport anisotropy in an A-type AFM bilayer system. (a) Schematic diagram of an A-type AFM bilayer system with the interlayer natural stacking. (b)–(d) Schematic band diagrams of a bilayer with the natural stacking. (b) Illustrative bands in the absence of external electric field. (c) When a vertical electric field is applied the spin degeneracy is lifted. (d) When the electric field is reversed the spin splitting is also opposite. (e) A bilayer with an interlayer twist angle of 90°. Carrier effective mass is different along two perpendicular axes, a and b, in each monolayer due to the different dispersion of the energy band along different directions, K_a and K_b, in momentum space (h). (f),(i) The layer and spin polarization and the dispersion of the energy band when a vertical electric field is applied, respectively. (g),(j) The opposite layer and spin splitting when the electric field is reversed.

CrSBr along two perpendicular axes a and b are calculated at the high symmetry points Γ in momentum space according to the dispersion of the energy band along different directions K_a and K_b.

III. RESULTS AND DISCUSSIONS

A. Design principle and physical mechanism

In Fig. 1(a) we schematically illustrate an A-type AFM bilayer with the intralayer FM order and interlayer AFM order. Without external electrical field, the layer and spin is degenerate due the AFM coupling between the upper layer and lower layer, as shown in Fig. 1(b). By applying a vertical electrical field, an electric potential difference between two layers is generated [16,17], lifting the layer degeneracy and spin degeneracy as shown in Fig. 1(c). When the electric field is reversed, the sign of spin polarization is also the opposite in Fig. 1(d). Therefore, a reversible spin polarization can be realized by electric field.

For materials with low structural symmetry, the electronic structure is often anisotropic. For example, the CrSBr monolayer has a strong in-plane anisotropy in the band structure. Thus, the carrier effective mass along two perpendicular crystal axis directions is different [28]. Such an anisotropy can be a tunable degree of freedom in the twisted bilayer system [29]. Based on two features of A-type AFM coupling and anisotropy of the carrier effective mass, we propose a general strategy to control the spin polarization and anisotropic carriers' transport properties by combining the interlayer twist and external electric field, as shown in Figs. 1(e)–1(j). A bilayer model with a twist angle of 90° is built, as shown in Fig. 1(e). In each monolayer, there is a huge difference of the carrier effective mass along the a and b axis due to the different dispersion of the energy band along different directions in momentum space [28], as shown in Fig. 1(h). For example, in the upper layer the carrier effective mass along a direction is larger than that along b direction, $m_a > m_b$, due to the steeper band along K_b direction. Since the lower layer has a twist angle of 90° relative to the upper layer, in the lower layer the carrier effective mass along a direction is smaller than that along b direction, $m_a < m_b$, due to the steep band along K_a direction. Thus, 90° rotation between the upper layer and lower layer induces a large difference of the carrier effective mass between two layers along the same crystal direction. When a vertical electric field is applied, the layer degeneracy can be lifted due to the induced electrostatic potential difference. When the positive electric field is applied, the VBM comes from the upper layer. Thus, the carrier effective mass along a direction is larger than that along b direction in the system, $m_a > m_b$, as shown in Figs. 1(f) and 1(i). When the electric field is reversed, the VBM comes from the lower layer. In this time, the carrier effective mass along a direction is smaller than that along b direction in the system, $m_a < m_b$, as shown in Figs. 1(g) and 1(j). Therefore, in an A-type AFM bilayer system with a twist angle of 90° the spin polarization and anisotropy of carrier effective mass can be simultaneously controlled by applying a vertical electric field to lift the layer degeneracy.

B. Electric field tuning of layer and spin polarization

In the following, we take bilayer CrSBr as an example to show the proposed strategy above. Recently, a FM semiconductor CrSBr [28,30–33] has brought widespread attention. Bulk CrSBr is a layered vdW AFM semiconductor, stable in air with low sensitivity, and can be easily separated along the direction perpendicular to the stack axis. Below its Néel temperature $T_N = 132$ K, CrSBr is an A-type AFM semiconductor with an intralayer FM and interlayer AFM coupling [30]. High carrier mobility and excellent dynamic and thermal stability makes it have great application potential in the future nanoelectronic devices.

Firstly, we study the A-type AFM bilayer CrSBr with the interlayer natural stacking. The top view and the side view of the atomic structure of the bilayer CrSBr are shown in Figs. 2(a) and 2(b), respectively. The optimized lattice constant is $a = 3.50$ Å and $b = 4.70$ Å, which agrees well with the experimental values [30]. Through translation optimization, we find the most stable stacking configuration in Fig. 2(b), which is consistent with the experimental measurement [30,34]. Magnetism comes mainly from the unfilled Cr-d orbitals in the twisted octahedron as shown in Fig. 2(c). In the unit cell of the bilayer CrSBr, there are two Cr atoms in each layer. We compare the energy of the four different magnetic configurations, and find that the A-type AFM configuration with the intralayer FM and interlayer AFM coupling is the most stable. This is also consistent with the experimental results [30,34]. In addition, we check the effects of stacking configuration and electric field on magnetic anisotropy. We find that the easy axis are all along the b direction for different stacking configurations, which is consistent with the experimental measurement [30] and theoretical calculations [33]. And the easy axis is also unchanged under the electric field, indicating the negligible electric field effect. Furthermore, we calculate the band structures with different magnetization direction a, b, and c. Similar band structures indicate that the spin and layer polarization does not depend on magnetization direction [26].

The band structures of A-type AFM bilayer CrSBr are shown in Figs. 2(d)–2(f). We find that the bilayer CrSBr is a semiconductor with an indirect gap of 0.98 eV in the absence of external electric field. The spin is degenerate due to the interlayer AFM coupling, as shown in Fig. 2(d). When a vertical electric field of 0.2 V/Å is applied, the electrostatic potential energy between the two layers becomes different and thus the spin degeneracy is

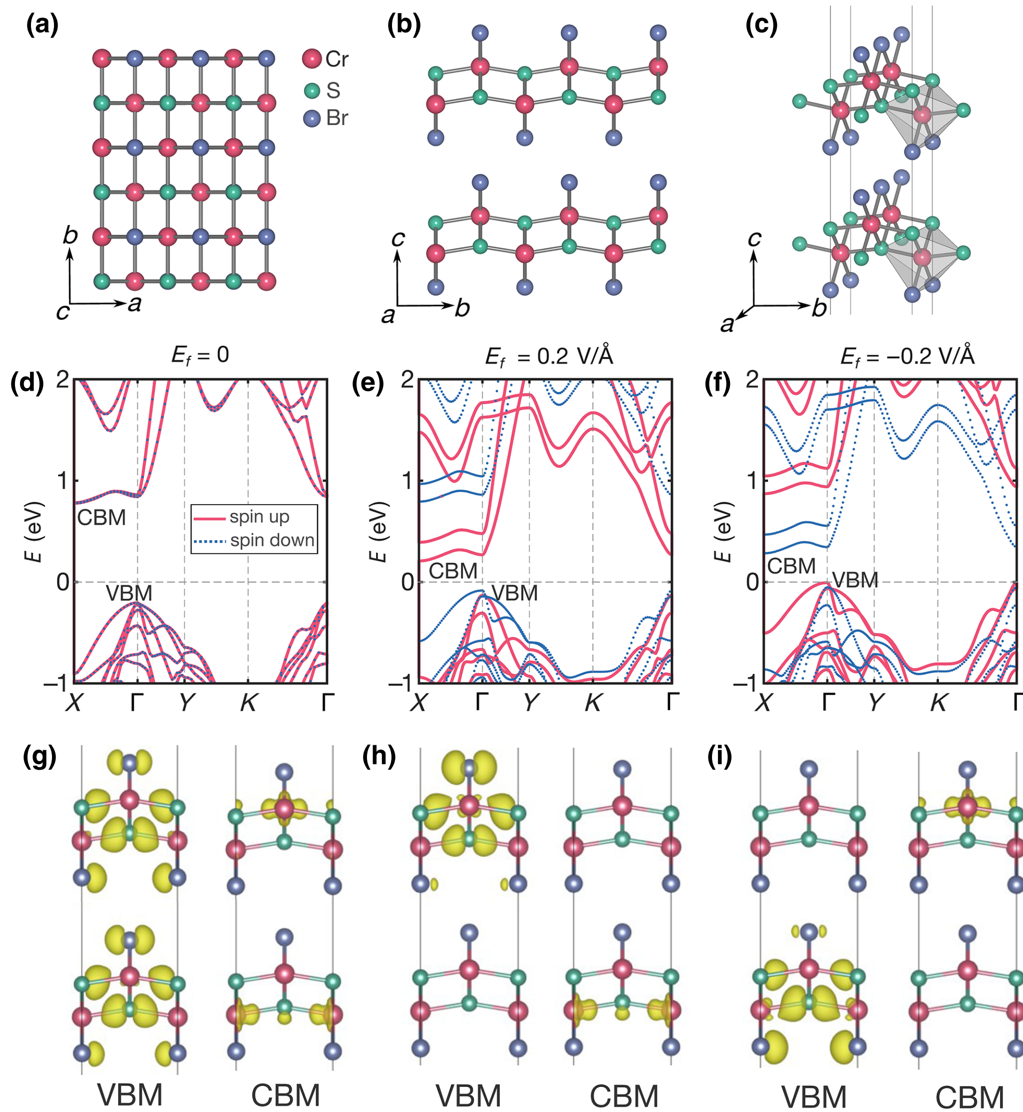

FIG. 2. Schematic diagram of the top (a) and side (b) views of the atomic structure of 2D bilayer CrSBr. (c) The twisted octahedron. Red, green, and blue represent Cr, S, and Br atoms, respectively. (d)–(f) Spin-polarized band structures of 2D A-type AFM bilayer CrSBr under the vertical electric field of 0 (d), 0.2 (e), and −0.2 V/Å (f). The red solid line and blue dashed lines represent the spin-up and spin-down channels, respectively. (g)–(i) Isosurface of the VBM and CBM charge density under the electric field of 0 (g), 0.2 (h), and −0.2 V/Å (i).

lifted, as shown in Fig. 2(e). It is noted that the band structures of bilayer CrSBr exhibit the typical characteristics of bipolar magnetic semiconductors [35] when an electric field is applied. In other words, the VBM and the conduction-band minimum (CBM) are contributed by the opposite spin-polarization states. When the electric field is reversed, the electron spin of the VBM and the CBM is also flipped, as shown in Fig. 2(f). This allows us to tune the spin polarization around the Fermi level by the electric field. Therefore, due to the electrostatic potential difference and A-type AFM coupling between the upper and lower layers, the spin degeneracy can be lifted, and the spin polarization can be controlled by applying a vertical electric field.

In addition, under an applied electric field, the electronic states at the VBM and the CBM do not only have the opposite spin direction, but also are localized in different layers, respectively, according to the layer polarization model in Fig. 1. The calculated charge-density isosurfaces of the VBM and the CBM are shown in Figs. 2(g)–2(i). In the absence of electric field, the electronic states from the VBM and CBM are layer degenerate in Fig. 2(g). When a positive vertical electric field is applied, the electronic states from the VBM and CBM are located, respectively, at the upper layer and lower layer since the layer degeneracy is lifted under the electric field, as shown in Fig. 2(h). When the electric field is reversed, the electronic states from the VBM and CBM are also spin reversed and

located, respectively, at the lower layer and upper layer in Fig. 2(i). In short, we can control the spin and layer degree of freedom simultaneously by applying a vertical electric field, which has potential applications in the spintronic devices.

C. Interlayer twist and electric field tuning of carrier effective mass anisotropy

Further, we turn to the study the tunable anisotropy of carrier effective mass in bilayer CrSBr with a twist angle of 90°. In Fig. 3(a), a bilayer CrSBr with a twist angle of 90° is shown. A 4×3 supercell is used to model this twisted system with a lattice mismatch of less than 1%. The reciprocal space geometry is shown in Fig. 4(b), in which the rectangular Brillouin zone (BZ) of the naturally stacked bilayer has been folded to the square-shaped BZ. We calculate the formation energy of the possible stacking configurations through interlayer translation [26]. Firstly, the negative formation energy indicates the stability of bilayer CrSBr. Secondly, the difference of formation energy is very tiny (<5 meV) for different translational configurations, indicating the small interlayer friction and easy interlayer slip at finite temperatures. Band-structure calculations indicate that the layer polarization and anisotropic band dispersion are robust for interlayer slip due to the weak interlayer interaction. Figures 3(c) and 3(d) show the electronic band structures of bilayer CrSBr with 0°and 90° twist angle. We find that the bilayer CrSBr with 90° twist angle becomes a direct band-gap semiconductor due to the band folding, and both VBM and CBM are located at Γ point in Fig. 3(d). In the natural stacking bilayer CrSBr, the spin is degenerate due to interlayer AFM coupling and the layer is also degenerate in absence of electric field. By contrast, after twisting 90° angle, the highest valence band (HVB) and lowest conduction band (LCB) show obvious anisotropy along the Γ-X and Γ-Y directions due to the interlayer twist, as shown in Fig. 3(d). Specifically, along the Γ-X direction, the HVB and LCB are contributed by the spin-down electron states from the lower layer, while along the Γ-Y direction the HVB and LCB are from the spin-up electron states in the upper layer. This originates from the anisotropic band structure and the change of symmetry caused by interlayer twist.

When a vertical electric field is applied, an electrostatic potential energy difference is generated between two layers. So, the energy bands contributed by the upper layer and lower layer will move towards low energy and high energy, respectively, as shown in Fig. 4(a). The VBM is contributed by the spin-up electronic states from the upper layer. The hole effective mass m_h along Γ-Y (a) direction is 4.19 m_0 (m_0 is the mass of a free electron), 35 times larger than 0.12 m_0 along Γ-X (b) direction, as shown in Fig. 4(c). When the electric field is reversed, the VBM

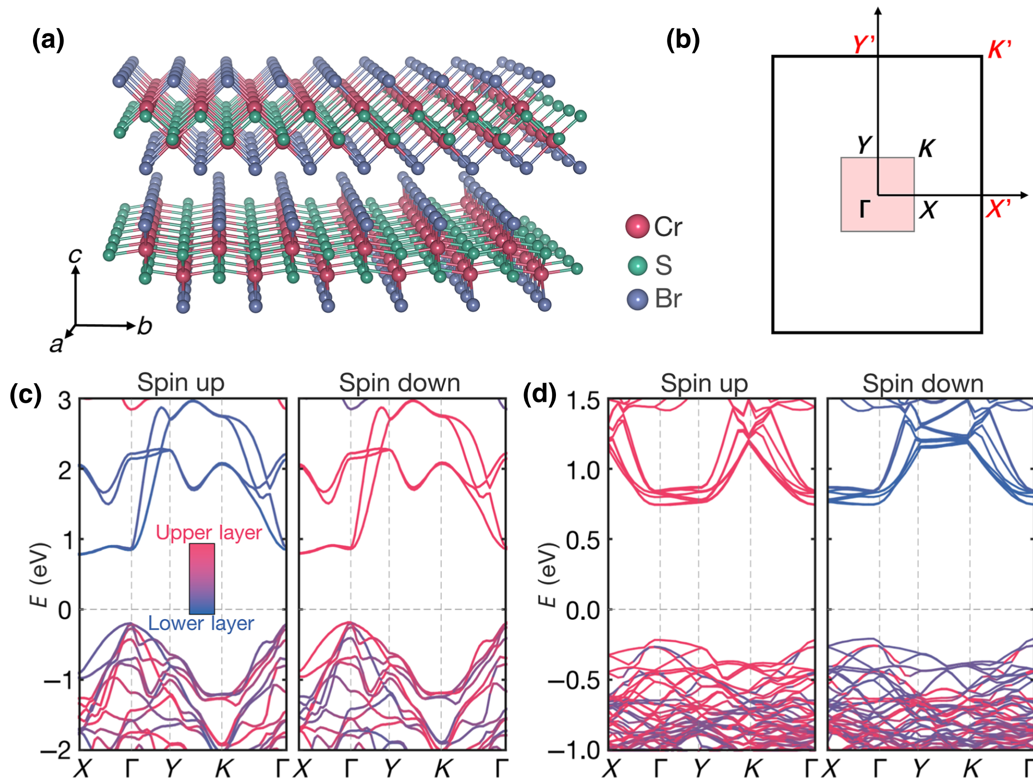

FIG. 3. (a) Side view of atomic structure and (b) Brillouin zone (shaded square) of 90° twisted bilayer CrSBr. (c),(d) Layer-projected and spin-polarized band structures of 0°(c) and 90° twisted (d) bilayer CrSBr.

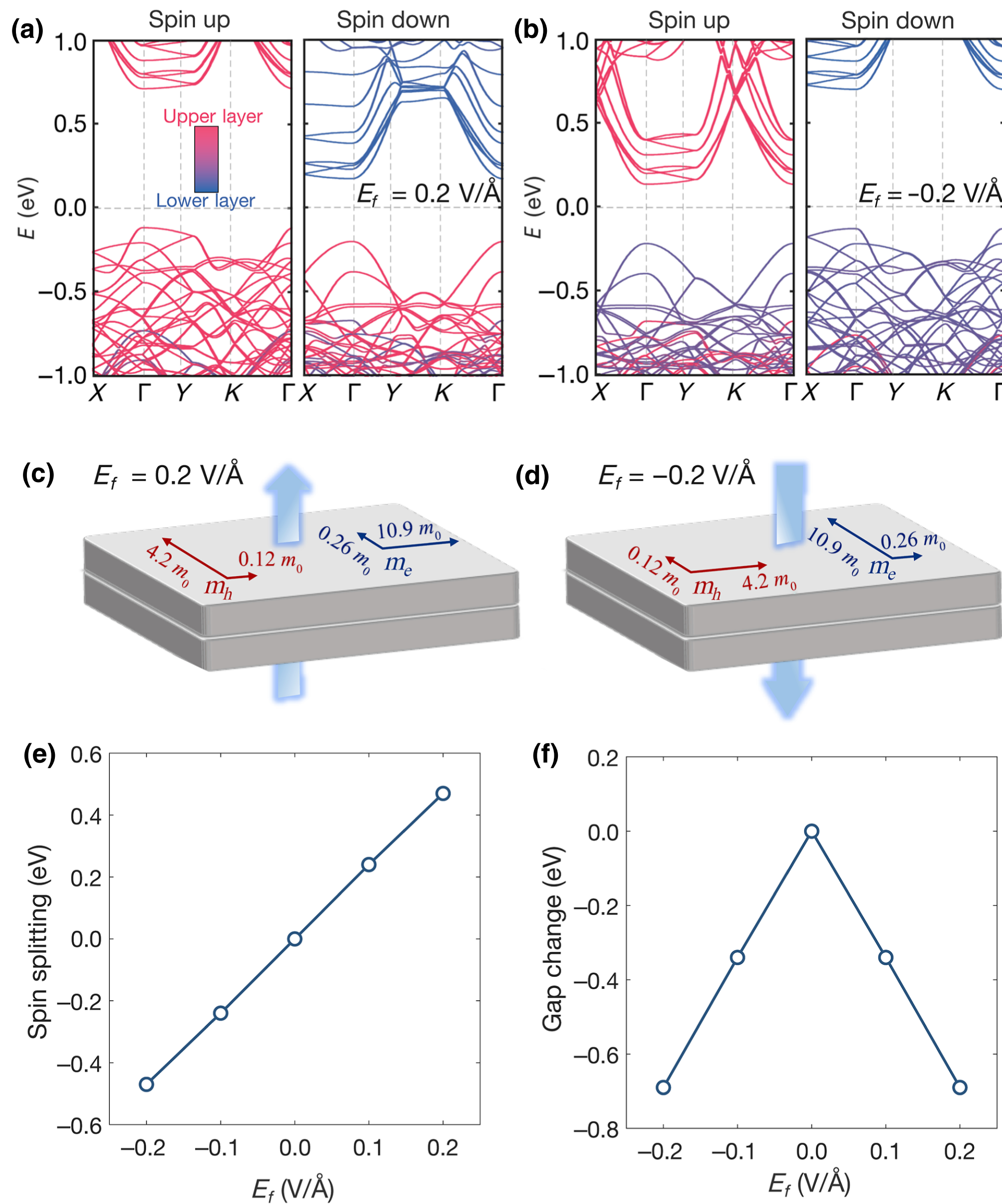

FIG. 4. (a),(b) The layer-projected and spin-polarized band structures of bilayer CrSBr with an interlayer twist angle of 90° under the vertical electric field of (a) 0.2 V/Å and (b) −0.2 V/Å. Red and blue represents the contribution of the upper layer and lower layer, respectively. (c),(d) Schematic representation of the electron and hole effective mass (m_e/m_h) of 2D bilayer CrSBr with an interlayer twist angle of 90° under the electric field of (c) 0.2 V/Å and (d) −0.2 V/Å. The unit is the mass m_0 of a free electron. (e) Variation of the spin splitting at the top of the valence band with the electric field for the 90° twisted bilayer CrSBr. (f) The variation of the band-gap change with the electric field for the 90° twisted bilayer CrSBr. Here, the band-gap change is defined as the difference between the band gap under the electric field and the band gap in the absence of electric field.

is contributed by the spin-down electronic states from the lower layer in Fig. 4(b). In this time, the hole effective mass along Γ-Y (a) direction is 0.12 m_0, smaller than 4.19 m_0 along Γ-X (b) direction, as shown in Fig. 4(d). For the electron effective mass m_e, there is a 42 times difference along different directions a and b. Electric-field-tunable spin polarization and anisotropy of electron effective mass is similar to a hole's, as shown in Figs. 4(c) and 4(d). Therefore, a vertical electric field can induce a hole (electron) effective mass that is 35 (42) times larger along one Cartesian axis than along the other axis, and the two axes can be exchanged by flipping the direction of electric field. In other words, we can rotate the spatial preference of the carrier-transport direction by 90° in a 2D plane by flipping the direction of electric field. So, besides the spin degree of freedom, anisotropy of carrier effective mass is also a

tunable degree of freedom in twisted bilayer CrSBr. These results indicate that the combination of the interlayer twist and electric field provides great flexibility to tune the spin polarization and anisotropic transport behavior of bilayer CrSBr.

It is noted that the spin polarization and effective mass can be controlled simultaneously in the A-type AFM CrSBr bilayer with 90° twist angle. Recently, the electrically controlled anisotropic carrier transport has been predicted theoretically in a black phosphorus bilayer with 90° twisted angle [29]. Due to the nonmagnetism of the black phosphorus bilayer, only the anisotropy of hole effective mass and optical transitions can be controlled by the electric field. However, in the A-type AFM CrSBr bilayer, by applying the electric field we cannot only control the preferred carrier transport direction, but also control the spin direction, realizing a multifunctional controllability. In addition, in order to show the dependence of the spin splitting on the electric field, we calculate the variation of the spin splitting at the top of the valence band with the electric field, as shown in Fig. 4(e). A linear dependence indicates the robustness of electric field control. The variation of the band-gap change with the electric field is also shown in Fig. 4(f). It indicates that under a wide range of electric fields, the system is still a semiconductor.

In addition, it is possible to make various bilayer configurations with different twist angles in the experiment. The unit cell of the CrSBr monolayer is orthorhombic, and the symmetry is low. From the perspective of theoretical simulation, the commensurate supercells of twisted bilayers are hard to find. As a comparison, within 1% mismatch we construct a CrSBr bilayer with twist angle of 21.6° and 348 atoms in a supercell [26]. Band structures under the electric field of 0.2 V/Å indicate that the anisotropic dispersion relation is still obvious for the highest valence band. Therefore, the layer polarization and anisotropic band dispersion are robust for interlayer twist.

Finally, we briefly discuss doping and half metallicity. By doping, we can make the Fermi level pass through the top of the valence band or the bottom of the conduction band, so as to realize the half metal. Atomic substitution doping is one of the most commonly used semiconductor-doping technologies to achieve permanent doping. The adjacent different main group elements can be selected to replace S or Br atoms. In addition, electrons and holes can also be doped by molecular adsorption. Since the outermost atoms are Br atoms in CrSBr, hole and electron doping can be realized by selecting molecules with stronger and weaker electronegativity.

IV. CONCLUSION

In summary, we propose a general strategy to realize the electric field control of spin and anisotropy of carrier effective mass in an A-type AFM bilayer system. By the first-principles calculations we study the A-type AFM bilayer CrSBr to show the validity of the principle. Firstly, the spin degeneracy can be lifted by applying a vertical electric field to generate an electrostatic potential difference between two layers. The spin polarization can be tuned by controlling the direction of electric field. Secondly, we study the A-type AFM bilayer CrSBr with an interlayer twist angle of 90° due to the in-plane anisotropic effective mass in each CrSBr monolayer. We find that both the spin direction and the carrier-transport anisotropy can be tuned simultaneously by applying a vertical electric field. This provides an alternative effective strategy for utilizing A-type AFM semiconductors to design spintronic devices by combining the interlayer twist and external electric field.

ACKNOWLEDGMENT

This work is supported by the National Natural Science Foundation of China (Project No. 11974148, 11804127) and Qing Lan Project in Jiangsu province.

CONFLICT OF INTEREST

The authors declare no competing financial interest.

[1] C. Tan, X. Cao, X. Wu, Q. He, J. Yang, X. Zhang, J. Chen, W. Zhao, S. Han, G. H. Nam, *et al.*, Recent advances in ultrathin two-dimensional nanomaterials, Chem. Rev. **117**, 6225 (2017).

[2] S. A. Wolf, D. D. Awschalom, R. A. Buhrman, J. M. Daughton, S. von Molnár, M. L. Roukes, A. Y. Chtchelkanova, and D. M. Treger, Spintronics: A spin-based electronics vision for the future, Science **294**, 1488 (2001).

[3] B. Huang, G. Clark, E. Navarro-Moratalla, D. R. Klein, R. Cheng, K. L. Seyler, D. Zhong, E. Schmidgall, M. A. McGuire, D. H. Cobden, *et al.*, Layer-dependent ferromagnetism in a van der Waals crystal down to the monolayer limit, Nature **546**, 270 (2017).

[4] C. Gong, L. Li, Z. Li, H. Ji, A. Stern, Y. Xia, T. Cao, W. Bao, C. Wang, Y. Wang, *et al.*, Discovery of intrinsic ferromagnetism in two-dimensional van der Waals crystals, Nature **546**, 265 (2017).

[5] C. Huang, J. Feng, F. Wu, D. Ahmed, B. Huang, H. Xiang, K. Deng, and E. Kan, Toward intrinsic room-temperature ferromagnetism in two-dimensional semiconductors, J. Am. Chem. Soc. **140**, 11519 (2018).

[6] K. S. Burch, Electric switching of magnetism in 2D, Nat. Nanotechnol. **13**, 532 (2018).

[7] Y. Zhang, J. Chu, L. Yin, T. A. Shifa, Z. Cheng, R. Cheng, F. Wang, Y. Wen, X. Zhan, Z. Wang, *et al.*, Ultrathin magnetic 2D single-crystal CrSe, Adv. Mater. **31**, 1900056 (2019).

[8] C. Gong and X. Zhang, Two-dimensional magnetic crystals and emergent heterostructure devices, Science **363**, 706 (2019).

[9] N. D. Mermin and H. Wagner, Absence of Ferromagnetism or Antiferromagnetism in One- or Two-Dimensional Isotropic Heisenberg Models, Phys. Rev. Lett. **17**, 1133 (1966).

[10] W. Zhang, P. K. J. Wong, R. Zhu, and A. T. Wee, Van der Waals magnets: wonder building blocks for two-dimensional spintronics?, InfoMat **1**, 479 (2019).

[11] K. F. Mak, C. Lee, J. Hone, J. Shan, and T. F. Heinz, Atomically Thin MoS_2: A New Direct-Gap Semiconductor, Phys. Rev. Lett. **105**, 136805 (2010).

[12] K. S. Novoselov, D. Jiang, F. Schedin, T. J. Booth, V. V. Khotkevich, S. V. Morozov, and A. K. Geim, Two-dimensional atomic crystals, Proc. Natl. Acad. Sci. USA. **102**, 10451 (2005).

[13] L. Li, Y. Yu, G. Ye, Q. Ge, X. Ou, H. Wu, D. Feng, X. Chen, and Y. Zhang, Black phosphorus field-effect transistors, Nat. Nanotechnol. **9**, 372 (2014).

[14] R. D. Dos Reis, M. G. Zavareh, M. O. Ajeesh, L. O. Kutelak, A. S. Sukhanov, S. Singh, J. Noky, Y. Sun, J. E. Fischer, K. Manna, *et al.*, Pressure Tuning of the Anomalous Hall Effect in the Chiral Antiferromagnet Mn_3Ge, Phys. Rev. Mater. **4**, 051401 (2020).

[15] N. Sivadas, S. Okamoto, and D. Xiao, Gate-Controllable Magneto-Optic Kerr Effect in Layered Collinear Antiferromagnets, Phys. Rev. Lett. **117**, 267203 (2016).

[16] S. Gong, C. Gong, Y. Sun, W. Tong, C. Duan, J. Chu, and X. Zhang, Electrically induced 2D half-metallic antiferromagnets and spin field effect transistors, Proc. Natl. Acad. Sci. USA. **115**, 8511 (2018).

[17] H. Lv, Y. Niu, X. Wu, and J. Yang, Electric-field tunable magnetism in van der Waals bilayers with A-type antiferromagnetic order: unipolar versus bipolar magnetic semiconductor, Nano Lett. **21**, 7050 (2021).

[18] Y. Zhu, Q. Cui, Y. Ga, J. Liang, and H. Yang, Anomalous valley Hall effect in A-type antiferromagnetic van der Waals heterostructures, Phys. Rev. B **105**, 134418 (2022).

[19] P. Hohenberg and W. Kohn, Density functional theory (DFT), Phys. Rev. **136**, B864 (1964).

[20] W. Kohn and L. J. Sham, Self-consistent equations including exchange and correlation effects, Phys. Rev. **140**, A1133 (1965).

[21] G. Kresse and J. Furthmüller, Efficient iterative schemes for ab initio total-energy calculations using a plane-wave basis set, Phys. Rev. B **54**, 11169 (1996).

[22] J. P. Perdew, K. Burke, and M. Ernzerhof, Generalized Gradient Approximation Made Simple, Phys. Rev. Lett. **77**, 3865 (1996).

[23] P. E. Blöchl, Projector augmented-wave method, Phys. Rev. B **50**, 17953 (1994).

[24] S. Froyen, Brillouin-zone integration by Fourier quadrature: Special points for superlattice and supercell calculations, Phys. Rev. B **39**, 3168 (1989).

[25] J. Hubbard, Electron correlations in narrow energy bands, Proc. R. Soc. London, Ser. A **276**, 238 (1963).

[26] See Supplemental Material at http://link.aps.org/supplemental/10.1103/PhysRevApplied.18.064086 for more information about the stacking configuratons, band structures with different magnetization direction, non-90° twist angle, formation energy, and band structures with different *U* values.

[27] S. Grimme, Semiempirical GGA-type density functional constructed with a long-range dispersion correction, J. Comput. Chem. **27**, 1787 (2006).

[28] H. Wang, J. Qi, and X. Qian, Electrically tunable high Curie temperature two-dimensional ferromagnetism in van der Waals layered crystals, Appl. Phys. Lett. **117**, 083102 (2020).

[29] T. Cao, Z. Li, D. Y. Qiu, and S. G. Louie, Gate switchable transport and optical anisotropy in 90 twisted bilayer black phosphorus, Nano Lett. **16**, 5542 (2016).

[30] E. J. Telford, A. H. Dismukes, K. Lee, M. Cheng, A. Wieteska, A. K. Bartholomew, Y. Chen, X. Xu, A. N. Pasupathy, X. Zhu, *et al.*, Layered antiferromagnetism induces large negative magnetoresistance in the van der Waals semiconductor CrSBr, Adv. Mater. **32**, 2003240 (2020).

[31] J. Klein, T. Pham, J. D. Thomsen, J. B. Curtis, T. Denneulin, M. Lorke, M. Florian, A. Steinhoff, R. A. Wiscons, J. Luxa, *et al.*, Control of structure and spin texture in the van der Waals layered magnet CrSBr, Nat. Commun. **13**, 5420 (2022).

[32] K. Lee, A. H. Dismukes, E. J. Telford, R. A. Wiscons, J. Wang, X. Xu, C. Nuckolls, C. R. Dean, X. Roy, and X. Zhu, Magnetic order and symmetry in the 2D semiconductor CrSBr, Nano Lett. **21**, 3511 (2021).

[33] K. Yang, G. Wang, L. Liu, D. Lu, and H. Wu, Triaxial magnetic anisotropy in the two-dimensional ferromagnetic semiconductor CrSBr, Phys. Rev. B **104**, 144416 (2021).

[34] J. Cenker, S. Sivakumar, K. Xie, A. Miller, P. Thijssen, Z. Liu, A. Dismukes, J. Fonseca, E. Anderson, X. Zhu, *et al.*, Reversible strain-induced magnetic phase transition in a van der Waals magnet, Nat. Nanotechnol. **17**, 256 (2022).

[35] X. Li and J. Yang, First-principles design of spintronics materials, Natl. Sci. Rev. **3**, 365 (2016).